THE ASTROPHYSICAL JOURNAL, 476:199–208, 1997 February 10

ALUMINUM OXIDE AND THE OPACITY OF OXYGEN-RICH CIRCUMSTELLAR DUST IN THE 12–17 MICRON RANGE

B. BEGEMANN, J. DORSCHNER, TH. HENNING, AND H. MUTSCHKE
Max-Planck-Gesellschaft, Arbeitsgruppe "Staub in Sternentstehungsgebieten," Schillergäßchen 3, D-07745 Jena, Germany
J. GÜRTLER AND C. KÖMPE
Universitäts-Sternwarte Jena, Schillergäßchen 2, D-07745 Jena, Germany
AND
R. NASS
Institut für Neue Materialien, Im Stadtwald, Geb. 43, D-66123 Saarbrücken, Germany
Received 1996 February 26; accepted 1996 September 3

ABSTRACT

Amorphous alumina (Al_2O_3) was produced by a sol-gel technique in order to make available its optical constants for possible astrophysical applications. Gradual annealing showed that the X-ray amorphousness of alumina ended somewhere between 723 and 873 K. Above this transition point, the structure changes into disordered γ-Al_2O_3. At $T > 1273$ K, crystalline α-Al_2O_3 (corundum) is formed.

Mie calculations show that amorphous alumina exhibits a wide Al-O vibrational band, peaking at 11.5–11.8 μm and having a steep "blue" and an extended "red" wing. It may be an important contributor to the continuous opacity between the silicate bands in oxygen-rich circumstellar envelopes, whereas it is ruled out for the explanation of the 13 μm band.

An average 13 μm band profile was derived from 51 *IRAS* low-resolution spectra of bright Mira stars and semiregular variables. Its shape, which is satisfactorily represented by a Lorentz profile, can be reproduced by Mie calculations with the data of α-Al_2O_3, but not with those of γ-Al_2O_3. The calculations show that the 13 μm band profile of α-Al_2O_3 is sensitive to grain shape. If α-Al_2O_3 is the absorber, a second band should be present at 21 μm.

A close correlation was found between the strengths of the 13 μm band and the 10 μm silicate band. It suggests that the 13 μm band carrier could also be somehow connected with silicate dust. Experimental arguments supporting this attribution are presented.

Subject headings: circumstellar matter — dust, extinction — infrared: ISM: lines and bands — stars: late-type

1. INTRODUCTION

The mid-infrared spectra of oxygen-rich circumstellar envelopes around many evolved stars are dominated by the silicate emission bands at about 10 and 19 μm. The *IRAS* low-resolution spectra (LRS) catalog (Olnon et al. 1986) presents the spectra of more than 1800 such sources. The wide range of widths and shapes and fine-structure details visible especially in the profile of the stronger 10 μm feature have formed the base for classification schemes, evolutionary characterization of the envelopes, and suggestions about the chemical and mineralogical properties of the silicatic dust (Vardya, de Jong, & Willems 1986; Little-Marenin & Little 1988, 1990; Ossenkopf, Henning, & Mathias 1992; Simpson 1991; Sloan & Price 1995). Parallel to these observationally based analyses, much laboratory work has been done on analogs that promise to reproduce the observed silicate band profiles, especially the 10 μm band profile (Krätschmer 1988; Gürtler, Henning, & Dorschner 1989; Koike & Tsuchiyama 1991; Koike, Shibai, & Tsuchiyama 1993; Jäger et al. 1994; Dorschner et al. 1995).

Much less attention has been paid to the spectral region between the silicate bands. In this very range, which we will refer to as "the trough" (12–17 μm), at least two points wait for their explanation and, therefore, deserve greater attention:

1. The opacity on the deepest point of the trough is surprisingly high, and the 19 μm band profile is rather shallow if compared with laboratory data of silicates (see Simpson 1991; Dorschner et al. 1995).

2. A weak but distinct emission band centered at about 13 μm was detected in the *IRAS* LRS spectra of Mira and other evolved giant stars (Vardya et al. 1986; Little-Marenin & Little 1988, 1990; Sloan, LeVan, & Little-Marenin 1996). Up to now, no satisfactory explanation has been put forward.

Possibly, both points are closely related in that the 13 μm band is only the visible "tip of the iceberg" and the continuum in the trough stems from the merging of a greater number of vibrational bands of solids condensing in the O-rich circumstellar environment. As promising candidates contributing to the emission in the 12–15 μm spectral range, Tielens (1990) suggested Al-containing framework silicates, SiO_2, aluminates, and metal oxides, among the latter aluminum oxide (Al_2O_3, alumina), spinel ($MgAl_2O_4$), aluminous cements, and rutile (TiO_2). However, most of these compounds have not yet been investigated seriously in an astrophysical context.

Since the 13 μm band has not been observed in carbon-rich stars, it was natural to attribute this feature to vibrations of an oxide, and Onaka, de Jong, & Willems (1989) tentatively identified it with the Al–O vibrational band of alumina grains. Glaccum (1995) suggested that sapphire (a terrestrial gem variety of Al_2O_3) could account for the 13 μm band. However, an ultimate proof of these identification proposals has been handicapped by the lack of a reliable

observationally based band profile.

Alumina (its rhombohedral modification is called corundum and designated as α-Al_2O_3) is considered as an early condensate in a cooling gas of solar composition. Numerous theoretical studies have been devoted to the sequence of condensation processes taking place in such environments as the early solar system, expanding envelopes around evolved stars, and supernova shells (Grossman & Larimer 1974; Lattimer, Schramm, & Grossman 1978; Kozasa & Hasagawa 1987; Sedlmayr 1989; Kozasa, Hasegawa, & Nomoto 1991). In his conception of the "chemical memory of the matter," Clayton (1982) stressed the important role that may be played by corundum and spinel crystallites. Because the are the innermost cores of oxidic supernova condensates (SUNOCONs) protected by a silicate mantle, they may transport the condensed SN-aluminum bonded within highly refractory compounds through the interstellar space. As a matter of fact, Al-enriched inclusions with isotopic anomalies (for Ca-Al inclusions, see McPherson, Wark, & Armstrong 1988) as well as micron-sized presolar corundum and spinel grains have been detected in primitive meteorites (Nittler et al. 1994, 1995; Huss et al. 1994; Hutcheon et al. 1994). The isotope signature points to a red giant and asymptotic giant branch (AGB) star origin of the corundum grains (Nittler et al. 1995). This lends additional support to the idea that alumina grains contribute to circumstellar dust opacity, even if the content of detectable corundum grains in the meteorites seems to be extremely small (about 0.5 ppm). There could be a large number of much smaller grains that escaped detection.

Optical constants of single crystals and microcrystalline particles of α-Al_2O_3 have been measured by many authors (Barker 1963; Loewenstein, Smith, & Morgan 1973; Toon, Pollack, & Khare 1976; Serna, Rendon, & Iglesias 1982; Gervais 1991). There are also measurements of other modifications of crystalline alumina, e.g., γ-Al_2O_3, an artificial product with cubic symmetry (Koike et al. 1995) and of amorphous alumina (Eriksson et al. 1981; Chu et al. 1988). All of these alumina samples exhibit bands coinciding nearly but not exactly with the peak position of the observed 13 μm band. The widths of the bands vary over a wide range. As for crystalline grains, one has to keep in mind that the calculated band position and profile is considerably influenced by surface modes.

From condensation theory, it can be expected that immediately after their condensation, alumina grains should be amorphous rather than crystalline (Sedlmayr 1989). The data of amorphous alumina available in the literature are not sufficient for an adequate description of the optical properties of such grains. The amorphous γ-Al_2O_3 by Eriksson et al. (1981) is not representative for amorphous alumina. The data set provided by Chu et al. (1988) suffers from the weakness of the absorption signal measured of the film on a sapphire substrate.

Therefore, we feel that measuring representative optical data of amorphous Al_2O_3 is very important for a general discussion of the possible contribution of alumina to the IR opacity in the circumstellar envelopes around oxygen-rich late-type stars, the understanding of the origin of the 13 μm band, and the solid-state structure of condensed circumstellar Al_2O_3 grains.

In this paper, which continues our efforts on oxides of possible astrophysical significance (see Henning et al. 1995), we wish to discuss the optical properties of amorphous and crystalline alumina particles and their relevance to the identification of the 13 μm band. Section 2 describes the preparation of amorphous alumina particles by sol-gel reactions, the phase transitions to crystalline modifications, and the derivation of the optical constants of amorphous alumina. Section 3 presents the extraction of the profile of the 13 μm band from *IRAS* LRS spectra, the comparison of all optical data available of Al_2O_3 with this profile, and alternative suggestions for the carrier of the 13 μm band.

2. OPTICAL PROPERTIES OF AMORPHOUS ALUMINA

2.1. *Preparation and Analytics*

The techniques of melting and quenching normally used in our laboratory for preparing amorphous refractory oxides (see, e.g., Begemann et al. 1995) fails in the case of aluminum oxide. Therefore, we applied the sol-gel technique commonly used in the material sciences for producing homogeneous amorphous solids (for details see, e.g., Brinker & Scherer 1990). This technique, which is totally different from the condensation process of Al_2O_3 in astrophysical environments, is exclusively used as an experimental trick to realize the totally amorphous structure. Since the astrophysical processes leading to the formation of solids are hardly understood in their details, in many cases the preparation of laboratory analogs aims only at producing a final product that is as similar as possible to the cosmic material regardless of the processes involved in the formation.

The Al_2O_3 gel was obtained by the reaction of aluminum secondary butoxide [$Al(OCHCH_3CH_2CH_3)_3$], ethylacetoacetate ($CH_3COCH_2COOC_2H_5$), propan-2-ol (C_3H_7OH), and demineralized water. After 6 months of stirring in order to reach maximum homogeneity, gelling was triggered by heat, and the resulting gel was dried. Separate samples of it were stepwise annealed in an oxygen stream at temperatures in the range $473 < T_{an} < 1773$ K. For each of these samples, density, IR transmission spectra in KBr and polyethylene (PE) embedding, and an X-ray diffractogram have been measured. For the samples of $T_{an} = 873$ and 1073 K, ^{27}Al-nuclear magnetic resonance (NMR) spectroscopy measurements have been carried out. In addition, the dried gel has been subjected to a differential thermal analysis (DTA) in an oxygen atmosphere as well as to differential thermogravimetry (TG).

Figure 1 shows a series of six mid-IR transmission spectra with increasing annealing temperature, which show characteristic spectral alterations. After drying at $T_{an} = 383$ K, the spectrum of the gel is dominated by bands of organic groups and water. During the annealing, the organics are oxidized and expelled as gases, and the respective bands disappear. The decompositional reactions are confirmed by the DTA results. The TG measurements show that the weight loss with increasing temperature reaches its endpoint at 689 K. We consider the spectrum for $T_{an} = 873$ K in Figure 1 to represent amorphous alumina. This spectrum shows a single broad Al–O vibrational band centered at about 13.9 μm. The amorphous state is verified by the X-ray diffraction pattern. The ^{27}Al-NMR spectrum shows three peaks at 6, 34, and 67 ppm, which are due to sixfold (octahedrally), "fivefold" (distorted tetrahedrally), and fourfold (tetrahedrally) coordinated aluminum, respectively. The coexistence of all coordinations of Al confirms the amorphous nature of the product.

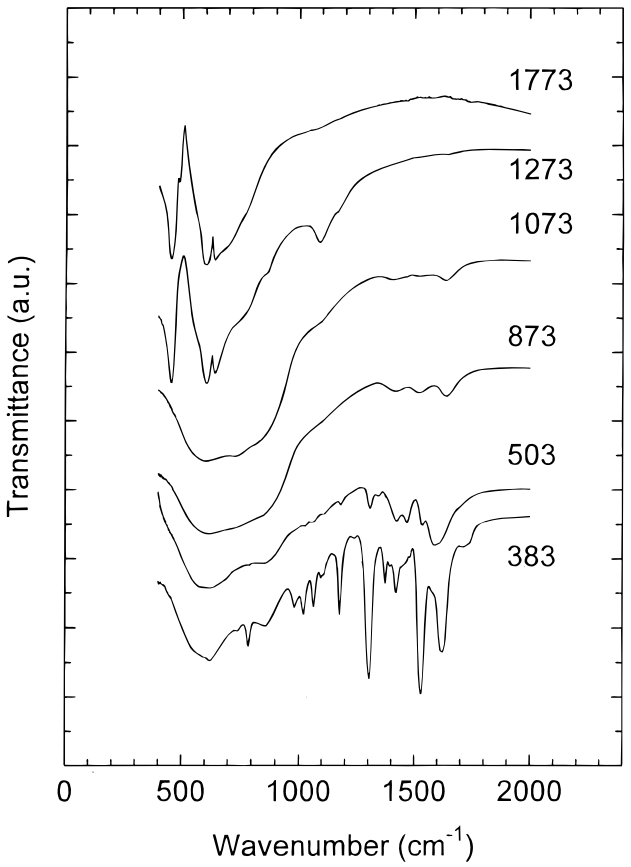

FIG. 1.—IR transmission spectra of Al_2O_3 samples in KBr (arbitrary units). The space between two long tick marks of the ordinate axis corresponds to 20% transmission. The samples were prepared by means of the sol-gel technique followed by annealing at the temperatures T_{an} = 383, 503, 873, 1073, 1273, and 1773 K. Note the occurrence of a second absorption band at about 460 cm^{-1} (21.7 μm) in the spectra of the high-temperature modification.

Above $T_{an} = 973$ the Al–O band in Figure 1 shows a weak splitting into two features with peaks at 16.7 and 13.7 μm. The number of broad Bragg reflection peaks in the X-ray diffraction patterns increases with growing temperature. At the same time, the peaks become sharper, which indicates increasing crystallinity. We consider the samples in the interval $973 \leq T_{an} \leq 1173$ K as representing disordered γ-Al_2O_3. This is supported by the X-ray diffraction measurements, from which the lattice constant of the 1173 K sample was estimated at 0.79 nm. In the NMR spectrum, the resonance of fivefold coordination of Al is no longer visible.

Crystalline γ-Al_2O_3 is characterized by the joint occurrence of six- and fourfold coordinated aluminum. The spectra of the samples with $T_{an} = 1273$ K are typical of α-Al_3O_3 (corundum). The transformation of amorphous γ-Al_2O_3 into crystalline α-Al_2O_3 is confirmed by the X-ray data and by an exothermic peak in the DTA curve.

Some additional weak IR bands for the samples with $723 \leq T_{an} \leq 1473$ K are due to H_2O (6.1 and 2.9 μm) and Al–OH (9.3, 7.1, and 6.6 μm). Aluminum oxide prepared by sol-gel technique contains a great number of micropores filled with adhesive water, which is difficult to remove by vacuum degasification.

2.2. *Determination of Optical Constants*

The optical constants of amorphous alumina have been determined on the 873 K sample. Its density $\rho = 2.45$ g cm^{-3} is considerably lower than those of crystalline γ-Al_2O_3 (3.5–3.9 g cm^{-3}) and α-Al_2O_3 (3.97 g cm^{-3}) (Hammond 1991). Based on TEM studies of a similar product by Yang, Pierre, & Uhlmann (1988), we consider porosity as the cause of the low density and assume that the pores are filled with liquid water. The density of the 873 K sample would imply a volume-filling factor of about $\frac{2}{3}$, if the density of the compact amorphous material has the plausible value of $\rho \approx 3.2$ g cm^{-3}.

For the spectroscopic measurements, small particles were produced by grinding the substance in an agate mortar. Sedimentation in acetone was used to separate grain size fractions smaller than 2 μm (coarse fraction) and 1 μm (fine fraction). The fine fraction was used for transmission spectroscopy in KBr embedding (mass ratio of 1:500, wavenumber range 400–5000 cm^{-1}), whereas the coarse fraction was embedded in PE (mass ratio 1:100; wavenumber range 20–650 cm^{-1}) for the FIR measurements. The alumina column densities in the PE and KBr pellets (diameter 1.27 cm, mass 200 mg) were 1.5 mg cm^{-2} and 0.3 mg cm^{-2}, respectively. The transmission of the pellets was measured by a Bruker 113v FTIR spectrometer using pure PE and KBr pellets as reference samples.

The measured mass absorption coefficients of both grain size fractions turned out to be in good agreement with each other in the overlap region (400–650 cm^{-1}). From the combined spectra, optical constants for amorphous alumina were derived for the range 20–1300 cm^{-1}. For this range, the particles have been sufficiently small to apply the Rayleigh approximation of the Mie formulae. Test calculations with continuous distributions of ellipsoids (CDE; see Bohren & Huffman 1983) confirmed that the influence of the particle morphology on the measured absorption band profile was sufficiently small for our amorphous alumina, so that the assumption of spherical grains was reasonable. Generally, shape effects on band profiles are weak as long as $\varepsilon' = n^2 - k^2 > -2 \times \varepsilon_m$ holds, where ε_m is the (real) dielectric constant of the transparent embedding medium.

The optical constants have been calculated by a Lorentz oscillator fit. For the high-frequency dielectric constant, we used the value $\varepsilon_\infty = 2.4$ as it follows from Bruggeman's mixing rule (see, e.g., Ossenkopf 1991) for a composite material consisting of a compact amorphous Al_2O_3 phase (2/3 per volume) with $\varepsilon_\infty = 2.8$ (Chu et al. 1988) and water-filled pores with $\varepsilon_\infty = 1.77$ (one-third). An adequate representation of the broad Al–O vibrational band was achieved by a superposition of eight Lorentz oscillators.

Table 1 lists the resulting n and k values, and Figure 2 compares our data with those determined by Chu et al. (1988), Eriksson et al. (1981), and Koike et al. (1995). These data sets represent materials of different states of order. The crystalline ISAS sample (Koike et al. 1995) shows the sharpest band profile, and our sol-gel product has the broadest feature (see Table 3), which suggests that our sample is more disordered than the thin film material studied by Eriksson et al. (1981). The increased imaginary part at wavelengths around 100 μm may be due to disorder-induced excitation of vibrational modes that cannot be optically excited in perfect crystalline materials.

The data for the porous material in Table 1 are "effective" optical constants since the material consists of alumina and water-filled pores. In order to estimate the influence of the porosity, we applied the Bruggeman mixing

TABLE 1

INFRARED OPTICAL CONSTANTS OF AMORPHOUS ALUMINA

	POROUS		COMPACT	
λ (μm)	n	k	n	k
7.8	1.328	0.063	1.343	0.078
8.0	1.312	0.068	1.323	0.086
8.2	1.296	0.075	1.301	0.095
8.4	1.278	0.082	1.277	0.105
8.6	1.259	0.090	1.251	0.116
8.8	1.239	0.099	1.223	0.129
9.0	1.217	0.110	1.193	0.144
9.2	1.192	0.122	1.160	0.162
9.4	1.166	0.137	1.124	0.183
9.6	1.136	0.156	1.084	0.208
9.8	1.104	0.178	1.041	0.240
10.0	1.070	0.208	0.994	0.281
10.2	1.033	0.247	0.944	0.334
10.4	0.999	0.300	0.896	0.408
10.6	0.976	0.368	0.862	0.504
10.8	0.974	0.442	0.859	0.612
11.0	0.991	0.509	0.886	0.712
11.2	1.016	0.563	0.927	0.792
11.4	1.045	0.612	0.977	0.861
11.6	1.079	0.650	1.036	0.913
11.8	1.112	0.678	1.092	0.946
12.0	1.139	0.700	1.138	0.969
12.5	1.196	0.751	1.224	1.016
13.0	1.249	0.795	1.294	1.059
13.5	1.299	0.834	1.355	1.098
14.0	1.345	0.868	1.408	1.135
14.5	1.386	0.901	1.455	1.176
15.0	1.429	0.939	1.505	1.227
15.5	1.479	0.976	1.567	1.278
16.0	1.535	1.007	1.638	1.322
16.5	1.594	1.031	1.715	1.356
17.0	1.654	1.048	1.795	1.382
17.5	1.716	1.059	1.877	1.398
18.0	1.778	1.060	1.962	1.402
18.5	1.838	1.052	2.044	1.392
19.0	1.893	1.034	2.118	1.369
19.5	1.939	1.010	2.182	1.336
20.0	1.976	0.981	2.236	1.298
21.0	2.019	0.927	2.298	1.220
22.0	2.036	0.889	2.318	1.165
23.0	2.043	0.872	2.323	1.143
24.0	2.053	0.873	2.332	1.149
25.0	2.071	0.886	2.355	1.171
26.0	2.103	0.901	2.400	1.197
27.0	2.143	0.912	2.459	1.217
28.0	2.190	0.913	2.528	1.223
29.0	2.236	0.906	2.598	1.214
30.0	2.278	0.891	2.664	1.193
32.0	2.346	0.848	2.772	1.128
34.0	2.391	0.800	2.844	1.051
36.0	2.418	0.758	2.891	0.978
38.0	2.435	0.723	2.919	0.915
40.0	2.446	0.696	2.938	0.861
45.0	2.463	0.655	2.955	0.763
50.0	2.477	0.636	2.949	0.699
60.0	2.513	0.630	2.941	0.654
70.0	2.557	0.640	2.948	0.672
80.0	2.606	0.652	2.987	0.704
90.0	2.657	0.662	3.043	0.728
100	2.708	0.670	3.103	0.742
125	2.828	0.675	3.254	0.755
150	2.931	0.661	3.385	0.747
175	3.017	0.639	3.501	0.712
200	3.091	0.612	3.599	0.668
250	3.197	0.552		
300	3.261	0.497		
400	3.342	0.411		
500	3.399	0.335		

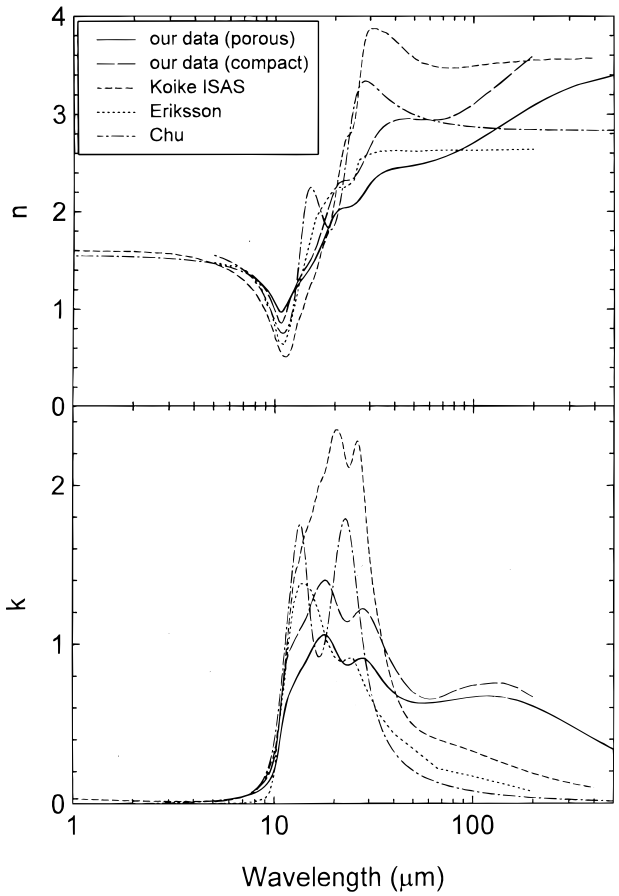

FIG. 2.—Real (n) and imaginary (k) parts of the refractive index of our amorphous Al_2O_3 (T_{an} = 873 K) compared with data of crystalline (Koike et al. 1995, sample ISAS) and amorphous γ-Al_2O_3 (Eriksson et al. 1981) and amorphous Al_2O_3 (Chu et al. 1988). For our material, we show the data of the original porous sample and data corrected for porosity by the Bruggeman theory ("compact material").

formula of effective medium theory. If the dielectric functions of the mixture and one component are known, the dielectric function of the other component can be deduced. The dielectric function of the water that filled the pores was taken from Hale & Querry (1973). The resulting data of the "compact material" are listed in Table 1 and plotted in Figure 2. As expected, they show a strengthened Al–O band.

3. COMPARISON WITH OBSERVATIONS AND DISCUSSION

3.1. *The 13 Micron Emission Profile of Late-Type Giants*

In the past, a critical examination of the identification of the 13 μm feature with alumina suffered both from the lack of adequate laboratory data and from the lack of a sufficiently accurate band profile derived from observational data. Therefore, we used the *IRAS* LRS catalog (Olnon et al. 1986) to derive an average 13 μm profile.

Since the 13 μm band was observed only in oxygen-rich stars, we selected all objects that belong to one of the LRS spectral classes 14–17, 2n, 4n, 6n, and 8n and have a 12 μm flux density $\geq$100 Jy. 338 objects were found. Many of their spectra show the 13 μm feature in emission. A source with a very distinct 13 μm band in the LRS spectrum is shown in Figure 3. The derivation of the band profile meets two main problems. The first one is presented by the LRS spectra that

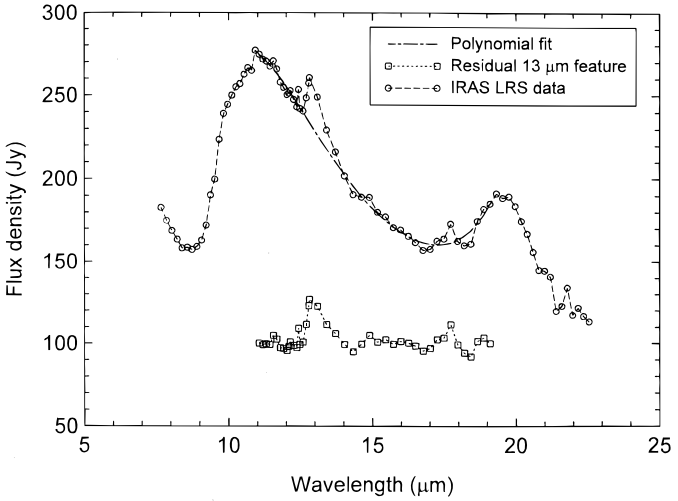

FIG. 3.—Illustration of the data reduction process using IRAS 07034−3551 as an example. Shown are the *IRAS* LRS data with the 10 μm and 13 μm features, the polynomial fit to the LRS data used to extract the 13 μm feature, and the residual 13 μm feature shifted by a value of 100 Jy.

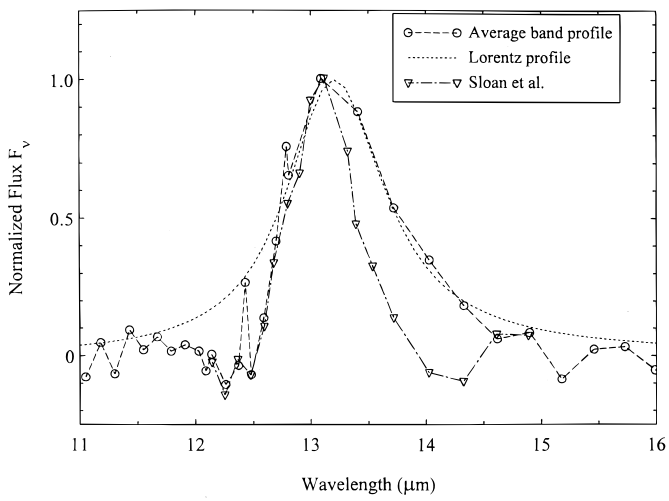

FIG. 4.—Profile of the 13 μm band based on the *IRAS* LRS spectra of the 51 stars listed in Table 2. A Lorentz profile and the profile derived by Sloan et al. (1996) are also shown.

consist of two independent parts that happen to overlap in the range of the 13 μm band. The profile of the band is thus certainly affected by how well the two parts of the spectra have been fitted together. In the worst case, a bad fitting could lead to a spurious 13 μm feature. The second problem is the subtraction of underlying dust emission, on which the 13 μm feature is superposed. This "background" consists of the broad 10 μm silicate emission feature and the contribution of the dust emission in the trough region between the two silicate features at 10 and 19 μm (see Fig. 3). Since the silicate spectra are different from source to source and the trough components are entirely unknown and since we do not know the temperature distribution of the circumstellar dust, it appears to be impossible to model the underlying "background" with sufficient certainty. Instead, we represented this emission by a fifth-degree polynomial. The exact shape of the polynomial obviously depends on the wavelength ranges of the data to which the polynomial is fitted. From our spectra with broad 10 μm features, we found that the polynomial should be fitted in the ranges from 11.05 to 12.48 μm and from 15.77 to 19.11 μm.

For deriving the 13 μm band profile, we selected 51 spectra for which we felt the polynomial fitted to these wavelength ranges provided a acceptable representation of the dust emission background. Consequently, all sources are excluded where the 10 μm silicate band is relatively narrow (e.g., IRAS 03507+1115 = IK Tau). An example illustrating our profile extraction procedure is given in Figure 3. Table 2 lists the 51 sources used to derive the average 13 μm profile. From these, 43 could be identified with variable stars (15 Mira stars, 26 semiregular variables, and two irregular variables). The average 13 μm profile is shown in Figure 4. According to our profile, the 13 μm band extends from about 12.25 to 15.2 μm. The peak position is 13.1 μm, and the width (FWHM) amounts to 1.05 μm. The band is clearly asymmetric. It can be fitted by a dispersion profile. Major discrepancies occur only around 12–12.5 μm where the scatter of the data points is particularly large. We consider the relatively good representation by a dispersion profile as evidence that our extraction procedure resulted in a physically reasonable band profile.

Sloan et al. (1996) independently obtained a profile of the 13 μm band from the *IRAS* LRS spectra of a larger sample of evolved variable stars by using a procedure similar to ours. These authors also carried out infrared observations and confirmed the 13 μm band seen in the *IRAS* LRS data. Their average profile is nearly symmetric, very narrow (FWHM = 0.6 μm), and peaks at 13.1 μm (see Fig. 4). Compared with our profile, there is excellent agreement on the blue side. The systematic deficit between 13.9 and 14.5 μm and the excess from 14.5–15.0 μm suggests that there are systematic differences between the dust emission and its representation by the polynomial. This could at least partly explain the smaller width of the profile derived by Sloan et al. (1996).

3.2. *Search for a 13 Micron Absorption Band*

In order to find out whether there are indications for the 13 μm feature in absorption, we inspected *IRAS* LRS spectra of bright sources with strong silicate absorption bands and found several objects with dips at the wavelength in question. The most promising cases are IRAS 17317−3331, 18257−1000, and 19283+1944.

Since aluminum is strongly depleted in the interstellar gas (Barker et al. 1984) and the missing atoms are assumed to be incorporated into dust grains, it makes sense to search for the 13 μm absorption band in the spectra of galactic sources behind heavily obscuring interstellar cloud complexes. An inspection of 8–13 μm spectra of Galactic center sources (Roche & Aitken 1985) that show a strong 10 μm silicate absorption band of the diffuse cloud dust yielded some positive indications. However, this finding must be viewed with some caution because the band is at the edge of the atmospheric window.

3.3. *Comparison of the Observationally Based 13 Micron Profiles with Laboratory Data of* Al_2O_3

An important test for the alumina hypothesis is the comparison of the profiles derived from the observations with theoretical profiles calculated with the optical constants of different samples of Al_2O_3.

Figure 5 shows theoretical profiles computed for different laboratory samples. We have plotted Q/a, where $4\pi a^2 Q$ is

TABLE 2

OBSERVATIONAL DATA

IRAS Name	Star Name	Var Type	Spectral Type	$S(13)$	S/N	$S(10)$
00192−2020.....	T Cet	SRc	M5–6 SIIe	11.5	4.7	44
00205+5530.....	T Cas	Mira	M6e–M9.0e	22.5	5.9	180
00245−0652.....	UY Cet	SRb	M7	10.3	5.8	51
01556+4511.....			M7 III	38.1	8.3	265
02192+5821.....	S Per	SRc	M3 Iae–M7	17.7	4.4	247
02427−5430.....	W Hor	SRb	MC	16.2	10.8	133
04020−1551.....	V Eri	SRc	M6 II	29.4	6.7	216
04166+4056.....	IR Per	SRa	M6.5	16.5	17.0	110
04387−3819.....	R Cae	Mira	M6e	7.3	4.4	86
05027−2158.....	T Lep	Mira	M6e–M9e	8.3	3.0	57
05132+5331.....	R Aur	Mira	M6.5e–M9.5e	13.2	9.4	167
06139+3313.....	VW Aur	SRb	M6	8.8	6.0	56
07034−3551.....			M6 III	22.2	8.6	176
08078−3801.....	AS Pup	Mira	M7e–M9	6.9	3.7	46
09185−4918.....	RW Vel	Mira	M7 III(II)e	11.8	9.4	96
09309−6234.....	R Car	Mira	M4e–M8e	12.5	5.5	150
09425+3444.....	R LMi	Mira	M6.5e–M9.0e	28.4	4.2	295
10562−6235.....				7.1	5.4	38
10580−1803.....	R Crt	SRb	M7	38.7	8.3	398
11461−3542.....	CD −35 7454		M7 III	23.1	5.6	189
12380+5607.....	Y UMa	SRb	M7 II–III:	8.0	3.5	77
13001+0527.....	RT Vir	SRb	M8 III	38.6	6.7	281
13269−2301.....	R Hya	Mira	M6e–M9eS(Tc)	91.7	5.1	638
13468+3947.....	R CVn	Mira	M5.5e–M9e	13.1	7.9	46
14003−7633.....	θ Aps	SRb	M7 III	39.3	8.2	297
14371+3245.....	RV Boo	SRb	M5e–M7e	6.4	3.3	55
15193+3132.....	S CrB	Mira	M6e–M8e	12.5	4.4	14
15410−0133.....	BG Ser	Mira	M6e–M8e	6.2	4.7	60
15492+4837.....	ST Her	SRb	M6–M7 IIIas	9.7	4.4	70
16306+7223.....	R UMi	SRb	M7 IIIe	6.1	4.2	41
16438−1133.....	V446 Oph	SR:	M8	9.9	6.3	7
16534−3030.....	RR Sco	Mira	M6 II–IIIe–M9	8.3	3.3	54
17102−1031.....	BD −07 4447		M7	11.8	4.2	145
17265−0725.....				7.6	4.6	82
18204−1344.....			M8	35.6	4.4	368
18359−0847.....	X Oph	Mira	M5e–M9e	15.3	4.6	131
19007−2247.....	SU Sgr	SRb	M6 III	5.5	4.4	41
19194+1734.....	T Sge	SRb	M4–M6.5	10.2	7.2	70
19510−5919.....	S Pav	SRa	M7 IIe–M8 III	27.7	8.9	188
20015+3019.....	V719 Cyg	Lb	M4e	11.5	4.0	174
20038−2722.....	V1943 Sgr	Lb	M8	15.9	4.5	118
20248+7505.....	UU Dra	SRb	M8 IIIe	14.2	6.8	97
20248−2825.....	T Mic	SRb	M6e	30.0	3.9	151
20431+1754.....	U Del	SRb	M5 II–III	7.4	4.3	78
20502+4709.....	RZ Cyg	SRa	M7.0–M8.2ea	10.1	7.7	83
21088+6817.....	T Cep	Mira	M5.5e–M8.8e	38.2	10.3	265
21439−0226.....	EP Aqr	SRb	M8 III	54.0	5.8	360
22035+3506.....	SV Peg	SRb	M7	17.8	6.6	132
22525+6033.....	MY Cep	SRc	M7–M7.5 I	10.1	5.8	85
22540−5740.....			M8 III	8.6	4.0	54
23365+5159.....	SV Cas	SRa	M6.5	9.4	5.3	99

NOTE.—$S(13)$ and $S(10)$ (in Jy) are the strengths of the 13 and the 10 μm band, respectively; S/N is the ratio of the 13 μm band strength to the r.m.s. scatter of the measured fluxes.

the extinction cross section of a particle with radius a. The ratio Q/a is related to the mass absorption coefficient κ by $\kappa = (3/4)(Q/a\rho)$, where ρ is the density of the grain material. The upper panel in Figure 5 shows the results for several amorphous samples. The particles are assumed to be spherical and much smaller than the wavelength (Rayleigh case). As discussed in § 2.2, for amorphous grains the optical properties are only weakly influenced by shape effects. The theoretical profiles of crystalline α-Al_2O_3 (Barker 1963) and γ-Al_2O_3 (Koike ISAS) are shown in the lower panel of Figure 5. Here we present calculations for both Rayleigh spheres and a CDE using a special weighing function (see Ossenkopf et al. 1992). Table 3 summarizes the band characteristics of our sample and those of other authors.

If we compare the wavelength position of the observed 13 μm band with the data in Table 3, we see that α-Al_2O_3 fits the observations best. In Figure 6, we plot the averaged observed 13 μm band together with theoretical profiles for our amorphous alumina and for α-Al_2O_3. For the calculations of the flux, we assume a grain temperature of 600 K. Rayleigh particles of α-Al_2O_3 produce a band that is too narrow compared with the observed one. The band broadens considerably if a CDE is assumed. Thus, it seems to be possible to reproduce the observed profile with the optical data of α-Al_2O_3, using an appropriate shape distribution of the grains. Moreover, profile variations among the stars could be easily accounted for by differing shape distributions.

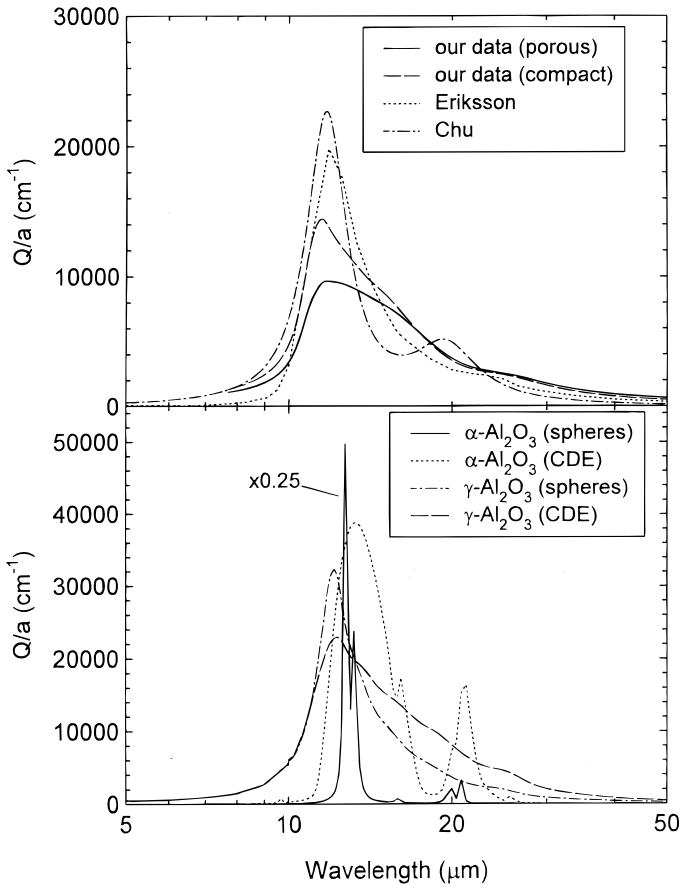

FIG. 5.—*Upper panel*: absorption coefficient Q/a calculated for spherical Rayleigh particles in vacuum for amorphous alumina data (this paper; Eriksson et al. 1981; Chu et al. 1988). *Lower panel*: absorption coefficient for spherical Rayleigh particles and a continuous distribution of ellipsoids (CDE) for the data of α-Al_2O_3 (Barker 1963; the profile for the spheres was scaled down by a factor of 0.25) and γ-Al_2O_3 (Koike et al. 1995, sample ISAS).

With the exception of that of crystalline α-Al_2O_3, all profiles in Figure 6 are much wider than the observed 13 μm profile. In particular, it is evident that the profile of amorphous alumina is not compatible with the observations. Therefore, we conclude that amorphous Al_2O_3 can be canceled from the list of candidate 13 μm band carriers.

A crucial test for the identification of the 13 μm band with Al–O vibrations of α-Al_2O_3 would be the detection of the

TABLE 3

BAND CHARACTERISTICS OF OUR SAMPLE AND THOSE OF OTHERS

Sample	λ_{peak} (μm)	FWHM (μm)	$Q_{ext}(\lambda_{peak})/a$ (cm^{-1})
This paper (porous)	11.8	8.0	9650
This paper (compact)	11.5	5.8	14450
Barker 1963: α-Al_2O_3	12.6	0.24	200000
Barker 1963: α-Al_2O_3 (CDE)	13.3	3.5	38800
Eriksson et al. 1981: γ-Al_2O_3	11.8	3.4	19850
Koike et al. 1995: ISAS	12.1	2.7	32400
Koike et al. 1995: ISAS (CDE)	12.3	6.5	23000
Chu et al. 1988: a-Al_2O_3	11.7	2.5	22700

NOTE.—Profile characteristics of the Al–O absorption band calculated for Rayleigh particles with the optical data of Table 2 and the published data of crystalline α- and γ-Al_2O_3 and amorphous alumina (a-Al_2O_3). The label "CDE" denotes calculations for a continuous distribution of ellipsoids (see text).

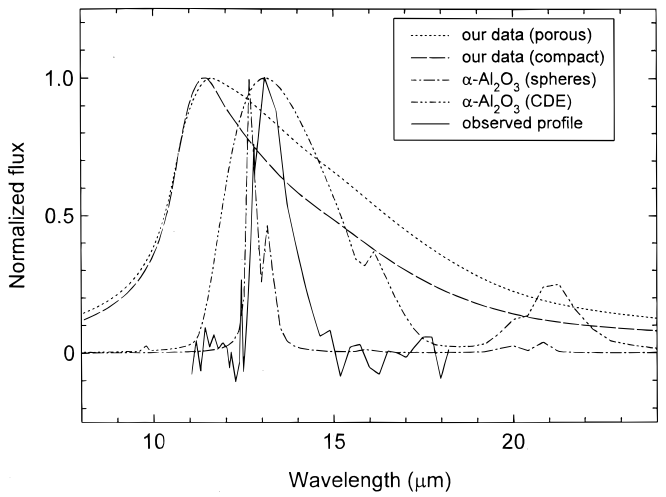

FIG. 6.—Comparison of the observed 13 μm profile (*solid line*) with theoretical flux calculated with our data and with those for α-Al_2O_3 (Barker 1963) for a dust temperature of 600 K.

second band at 21 μm (see Fig. 5, *lower panel*). The strength of this band is 42% of that of the 13 μm band for grains with a CDE and much smaller for spherical ones. Since the observed width of the 13 μm band lies somewhere between the predictions for the CDE and Rayleigh cases, we expect the same for the observed strength of a possible 21 μm feature. Inspection of the *IRAS* LRS spectra of those objects in Table 2 that exhibit the strongest 13 μm bands did not give convincing evidence for the 21 μm band. Better data, such as, e. g., *ISO* may provide, are clearly needed to decide this matter.

The observed strengths of the 13 μm and of the silicate bands are closely correlated as shown in Figure 8. The observed ratio is about 0.13. Adopting 39,000 cm^{-1} and 3000 cm^{-1} for the absorption coefficient of α-Al_2O_3 and silicate grains, respectively, and a Al/Si abundance ratio of about 10 (Palme & Beer 1993), we estimate a band ratio of 0.51, if all of the Al atoms were locked up in α-Al_2O_3 grains. Thus, about 25% of the available aluminum is needed in form of crystalline alumina grains to account for the 13 μm band.

The present concept of grain formation in extended stellar atmospheres (Sedlmayr 1989) states that newly formed grains are amorphous rather than crystalline. If the identification of the 13 μm band with α-Al_2O_3 is correct, a significant fraction of the originally amorphous alumina grains must pass through some crystallization process. This may be part of the evolutionary process of alumina grains and requires that they remain hot enough for a sufficiently long time. Possibly, the crystallization process cannot take place in every circumstellar envelope, which may explain why the 13 μm band is absent in some spectra.

If most of the available aluminum is in the form of the amorphous oxide, then amorphous alumina, like our laboratory analog product, should be one of the main absorbers in the trough region between the silicate bands. A simple estimate shows that the trough opacity of a laboratory analog, e.g., $MgFeSiO_4$-glass (see Dorschner et al. 1995), should be enhanced by 30%, if we assume that all Si and Al atoms are bonded in silicate and alumina, respectively, and if the band strength of our compact amorphous Al_2O_3 is correct.

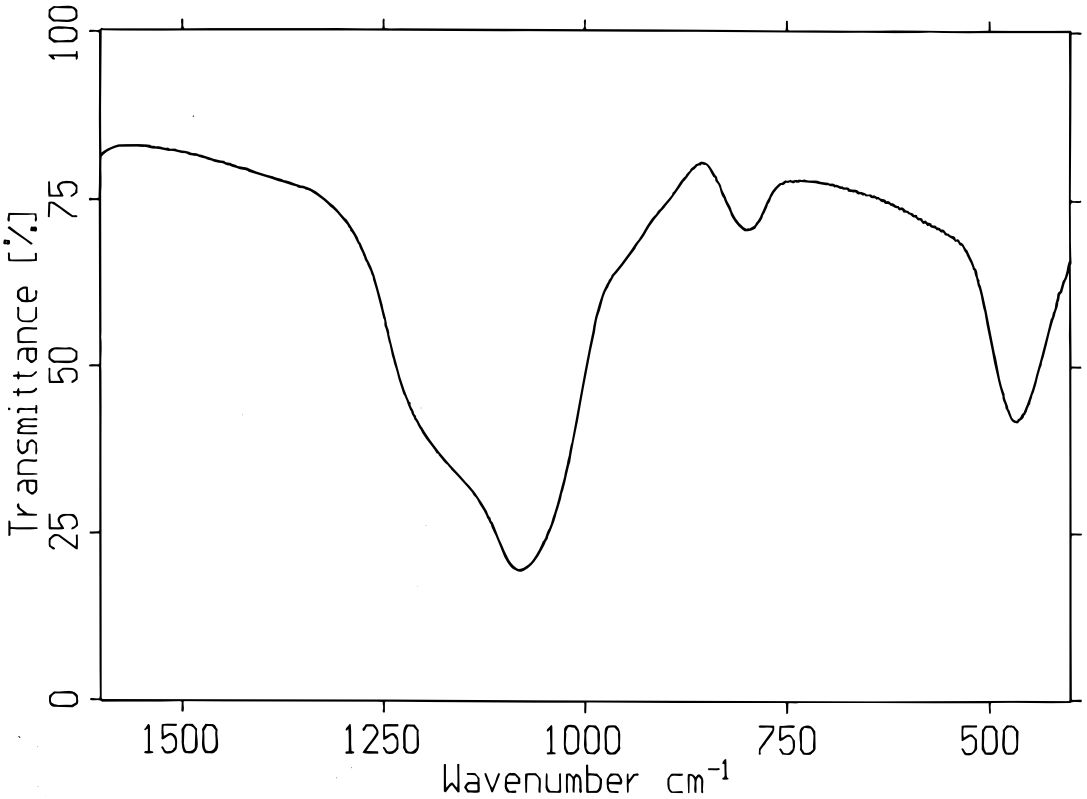

FIG. 7.—Transmission spectrum of small grains of an amorphous Mg silicate produced by sol-gel techniques. The composition can be given by the sum formula $Mg_{0.7}SiO_{2.7}$.

Apart from Al_2O_3, further Al-containing absorbers could contribute to the trough opacity. Discussing mineralogical implications of the *IRAS* LRS spectra, Tielens (1990) stressed the role of aluminum bonded in framework silicates and oxidic compounds for the wavelength range 12–17 μm. In a recent experimental study, Mutschke et al. (1997) confirmed that alumino-silicate glasses show an absorption band peaking in the range 13–14 μm. Further, spinel ($MgAl_2O_4$; optical constants by Tropf & Thomas 1991a), ferrospinel ($FeAl_2O_4$ = hercynite), and aluminum oxynitride (ALON; optical constants by Tropf & Thomas 1991b) could be added to the list of potential trough absorbers of astrophysical significance.

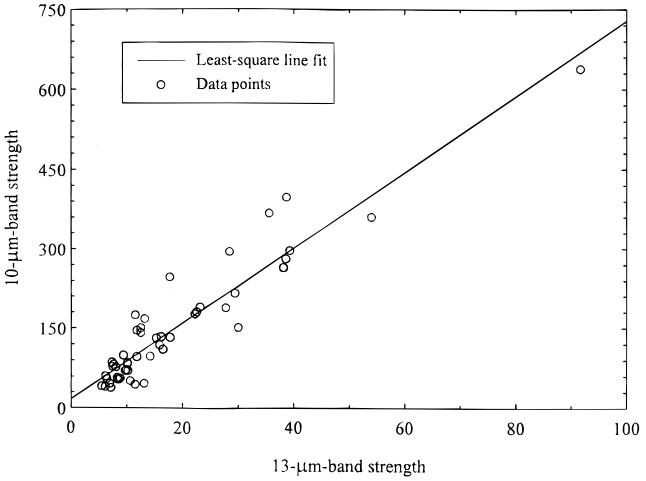

FIG. 8.—Correlation between the band strengths (in Jy) of the 10 and 13 μm bands for the 51 sources listed in Table 2. The correlation coefficient is 0.94 and the ratio of the 10 μm to the 13 μm band strength is 7.65.

3.4. *Alternative Explanations of the 13 Micron Band: The Case for Silicates*

Although there are, at present, no convincing arguments against aluminum compounds as absorbers in the range 12–17 μm, alternative interpretations remain attractive. Here, we suggest that the 13 μm band could be related to silicates. Vardya et al. (1986) were the first who attributed this band to an "Al/Ca silicate." It has also been noted that feldspar minerals generally show a weak feature near 13 μm. In these solids, Si is substituted partially by Al, and this feature is due to Al–O vibrations.

However, some silicates show bands in the 13 μm region without containing aluminum. Raman spectroscopic investigations suggest that silica and silicate glasses could have vibrational bands in the trough region. For instance, a band at 12.5 μm occurs in silica glass spectra and a band between 14 and 17 μm in spectra of CaO-MgO-SiO_2 and $CaMgSiO_4$-SiO_2 glass systems, the precise position depending on the metal-to-SiO_2 ratio (McMillan 1984). Some of these bands are also IR-active.

Spectra of pyroxene glasses, which were thoroughly studied in Jena (Dorschner, Gürtler, & Henning 1989; Jäger et al. 1994), show an unusually flat trough bottom pointing to additional absorption components, which, in the case of salite glass [$Ca(Mg, Fe)Si_2O_6$], becomes visible as a small peak at about 13.5 μm. Furthermore, experiments in progress (Begemann et al. 1997) indicate that amorphous Mg-Fe silicates prepared by sol-gel techniques show a distinct band at about 12.5 μm with the precise position and strength depending on the cation ratio (Fig. 7).

If the observed 13 μm band is indeed due to a vibration within the silicate structure, then the strengths of the observed 13 μm band should necessarily correlate with

those of the 10 μm band. Such a correlation was found with our observational material, from which the 13 μm band profile was derived. In Figure 8, this relationship is shown. The correlation coefficient for our sample of 51 sources amounts to 0.94. A natural explanation for this correlation would be the assumption of a silicate origin of the 13 μm band. If the band ratios of the amorphous silicate shown in Figure 7 are comparable with those of circumstellar silicates, then the relative strength of this minor band in the trough region would be consistent with its silicate origin. Obviously, this particular silicate is not a perfect laboratory analog of the circumstellar silicate because the wavelength position does not match exactly the observed 13 μm band.

A third silicate band would provide additional mineralogical information on the circumstellar and interstellar dust silicates. A difficulty with this interpretation is that the presence of the 13 μm band seems not to correlate with profile characteristics of the other silicate bands. Further investigations are necessary to clarify this point.

4. SUMMARY AND CONCLUSIONS

In the spectra of many oxygen-rich AGB stars with strong circumstellar silicate emission bands, there is a weak but distinct emission band at about 13 μm wavelength. In this paper, we have studied whether this band could be due to Al–O vibrations in crystalline and/or amorphous alumina grains, as was suggested in the literature. Since under the nonequilibrium conditions in the circumstellar environment the formation of amorphous solids is expected, we have studied amorphous Al_2O_3 produced by sol-gel reactions. Optical constants have been reported both for the original porous substance and for a "compact" material, the properties of which were derived by applying effective medium theory. Mie calculations suggest that small grains of amorphous alumina should show a very broad band peaking at 11.5 and 11.8 μm for the compact and the porous material, respectively.

We have derived a new profile of the 13 μm band from *IRAS* LRS spectra of a sample of very bright AGB stars. We found this profile to be similar to a dispersion profile. After completing the analysis, we learned of similar work by Sloan et al. (1996). Their band profile is considerably narrower than ours, which may be attributed to a somewhat different subtraction of the underlying silicate emission.

From a comparison of the observed profile with the results of the Mie calculations, we conclude that amorphous alumina grains cannot account for the 13 μm band seen in the mid-IR spectra of circumstellar oxygen-rich envelopes. However, such grains can contribute to the generally high level of emission in the region between the two silicate bands. Therefore, they have to be considered as a probably important opacity source for model calculations of circumstellar envelopes. The reproduction of the observed 13 μm band profile may be possible with the data of crystalline α-Al_2O_3, if one takes into account that the shapes of the particles play a decisive role for the band profile. Strong support for the identification of the 13 μm band by α-Al_2O_3 would come from the detection of a weak band at 21 μm. In the *IRAS* LRS spectra of our 13 μm sources, we did not find convincing evidence for its presence. We encourage observers to search for this band, e.g., in the *ISO* spectra.

We found a close correlation of the strength of the 13 μm band with that of the 10 μm silicate band. The observed band ratio is in agreement with an aluminum abundance as found in the Sun and the chondrites. Nevertheless, it seems reasonable to consider other carriers of the 13 μm band as well. We suggest that silicates themselves could be promising candidates.

We should like to thank Elke Wagner, Institut für Glaschemie der Friedrich-Schiller-Universität Jena, for carrying out the X-ray diffractometry; Thomas Stelzner, Institut für Geowissenschaften der Friedrich-Schiller-Universität Jena, for the DTA measurements; Wilfried Hoffbauer, Institut für Anorganische Chemie der Universität Bonn for the NMR measurements; Ute Bai, Institut für Neue Materialien, Saarbrücken, and Gabriele Born, MPG-Arbeitsgruppe "Staub in Sternentstehungsgebieten," Jena, for the preparatory work; and Walter Teuschel, MPG-Arbeitsgruppe "Staub in Sternentstehungsgebieten," Jena, for spectroscopic measurements. We are grateful to Irene Little-Marenin, Wellesley College, for making available to us her work on the 13 μm feature before publication. One of us (B. B.) gratefully acknowledges the hospitality of the Institut für Neue Materialien in Saarbrücken, Germany. This project has been partially supported by the German Bundesministerium für Bildung, Wissenschaft, Forschung und Technologie (Förderkennzeichen 05 2JN13A).

REFERENCES

Barker, A. S., Jr. 1963, Phys. Rev., 132, 1474
Barker, E. S., Lugger, P. M., Weiler, E. J., & York, D. G. 1984, ApJ, 280, 600
Begemann, B., Dorschner, J., Henning, Th., & Mutschke, H. 1997, in preparation
Begemann, B., Henning, Th., Mutschke, H., & Dorschner, J. 1995, Planet. Space Sci., 43, 1257
Bohren, C. F., & Huffman, D. R. 1983, Absorption and Scattering of Light by Small Particles (New York: John Wiley & Sons)
Brinker, C. J., & Scherer, G. W. 1990, Sol-Gel Science (San Diego: Academic)
Clayton, D. D. 1982, QJRAS, 23, 174
Chu, Y. T., Bates, J. B., White, C. W., & Farlow, G. C. 1988, J. Appl. Phys., 64, 3727
Dorschner, J., Begemann, B., Henning, Th., Jäger, C., & Mutschke, H. 1995, A&A, 300, 503
Dorschner, J., Gürtler, J., & Henning, Th. 1989, Astron. Nachr., 310, 303
Eriksson, T. S., Hjortsberg, A., Niklasson, G. A., & Granqvist, C. G. 1981, Appl. Optics, 20, 2742
Gervais, F. 1991, in Handbook of Optical Constants of Solids II, ed. E. D. Palik (Boston: Academic), 761
Glaccum, W. 1995, in ASP Conf. Proc. 73, Airborne Astronomy Symposium on the Galactic Ecosystem: From Gas to Stars to Dust, ed. M. R. Haas, J. A. Davidson, & E. F. Erickson (San Francisco: ASP), 395
Grossman, L., & Larimer, J. W. 1974, Rev. Geophys. Space Phys., 12, 71
Gürtler, J., Henning, Th., & Dorschner, J. 1989, Astron. Nachr., 310, 319
Hale, G. M., & Querry, M. R. 1973, Appl. Opt., 12, 555
Hammond, C. R. 1991, in CRC Handbook of Chemistry and Physics, ed. D. R. Lide (71st ed.; Boca Raton: CRC Press) 4-41
Henning, Th., Begemann, B., Mutschke, H., & Dorschner, J. 1995, A&AS, 112, 143
Huss, G. R., Fahey, A. J., Gallino, R., & Wasserburg, G. J. 1994, ApJ, 430, L81
Hutcheon, I. D., Huss, G. R., Fahey, A. J., & Wasserburg, G. J. 1994, ApJ, 425, L97
Jäger, C., Mutschke, H., Begemann, B., Dorschner, J., & Henning, Th. 1994, A&A, 292, 641
Koike, C., Kaito, C., Yamamoto, T., Shibai, H., Kimura, S., & Suto, H. 1995, Icarus, 114, 203
Koike, C., Shibai, H., & Tsuchiyama, A. 1993, MNRAS, 264, 654
Koike, C., & Tsuchiyama, A. 1991, in Origin and Evolution of Interplanetary Dust, ed. A. C. Levasseur-Regourd & H. Hasegawa (Dordrecht: Kluwer), 95
Kozasa, T., & Hasegawa, H. 1987, Prog. Theor. Phys., 77, 1402
Kozasa, T., Hasegawa, H., & Nomoto, K. 1991, A&A, 249, 474
Krätschmer, W. 1988, in Experiments on Cosmic Dust Analogues, ed. E. Bussoletti, C. Fusco, & G. Longo (Dordrecht: Kluwer), 95
Lattimer, I. M., Schramm, D. N., & Grossman, L. 1978, ApJ, 219, 230

Little-Marenin, I. R., & Little, S. J. 1988, ApJ, 333, 305
———. 1990, AJ, 99, 1173
Loewenstein, E. V., Smith, D. R., & Morgan, R. L. 1973, Appl. Opt., 12, 398
McMillan, P. 1984, Am. Mineralogist, 69, 645
McPherson, G. J., Wark, D. A., & Armstrong, J. D. 1988, in Meteorites and the Early Solar System, ed. J. F. Kerridge & M. S. Matthews (Tucson: Univ. Arizona Press), 746
Mutschke, H., Begemann, B., Dorschner, J., & Henning, Th. 1997, in preparation
Nittler, L. R., Alexander, C. M. O'D., Gao, X., Walker, R. M., & Zinner, E. K. 1994, Nature, 370, 443
———. 1995, in Nuclei in the Cosmos, ed. M. Busso, R. Gallino, & C. M. Raiteri (New York: AIP), 563
Olnon, F. M., Raimond, E., Neugebauer, G., van Duinen, R. J., & Habing, H. J. 1986, A&AS, 65, 607
Onaka, T., de Jong, T., & Willems, F. J. 1989, A&A, 218, 169
Ossenkopf, V. 1991, A&A, 251, 210
Ossenkopf, V., Henning, Th., & Mathis, J. S. 1992, A&A, 261, 567
Palme, H., & Beer, H. 1993, in Landolt-Börnstein/New Series, Group VI, Vol. 3, Astronomy and Astrophysics, Extension and Supplement to Vol. 2, ed. H. H. Voigt (Berlin: Springer), 202
Roche, P. F., & Aitken, D. K. 1985, MNRAS, 215, 425
Sedlmayr, E. 1989, in Interstellar Dust, ed. L. J. Allamandola & A. G. G. M. Tielens (Dordrecht: Kluwer), 467
Serna, C. J., Rendon, J. L., & Iglesias, J. E. 1982, Spectrochim. Acta., 38A, 797
Simpson, J. P. 1991, ApJ, 368, 570
Sloan, G. C., LeVan, P. D., & Little-Marenin, I. R. 1996, ApJ, 463, 310
Sloan, G. C., & Price, S. D. 1995, ApJ, 451, 758
Tielens, A. G. G. M. 1990, in From Miras to Planetary Nebulae, ed. M. E. Mennessier & A. Omont (Gif-sur-Yvette: Editions Frontières), 186
Toon, O. B., Pollack, J. B., & Khare, B. N. 1976, J. Geophys. Res., 81, 33
Tropf, W. J., & Thomas, M. E. 1991a, in Handbook of Optical Constants of Solids II, ed. E. D. Palik (Boston: Academic), 883
———. 1991b, in Handbook of Optical Constants of Solids II, ed. E. D. Palik (Boston: Academic), 777
Vardya, M. S., de Jong, T., & Willems, F. J. 1986, ApJ, 304, L29
Yang, X., Pierre, A. C., & Uhlmann, D. R. 1988, J. Non-Cryst. Solids, 100, 371